

Beijing National
Tandem Accelerator Laboratory

ANNUAL REPORT

2005

China Institute of Atomic Energy

Atomic Energy Press

Beijing National
Tandem Accelerator Laboratory

ANNUAL REPORT

2005

China Institute of Atomic Energy

Atomic Energy Press

图书在版编目(CIP)数据

北京串列加速器核物理国家实验室 2005 年报: 英文/北京串
列加速器核物理国家实验室编. —北京: 原子能出版社,
2007. 2

ISBN 978-7-5022-3875-9

I. 北… II. 北… III. ①核物理学—研究—中国—2005—
年报②串列式加速器—研究—中国—2005—年报—英文 IV.
0571-54 TL52-54

中国版本图书馆 CIP 数据核字 (2007) 第 022926 号

Annual Report for Beijing National Tandem Accelerator Laboratory (2005)

Published by Atomic Energy Press, P. O. Box 2108, Postcode: 100037, Beijing, China

Printed by Printing House of WenLian in China

Format: 880 mm×1 230 mm 1/16

First Edition in Beijing, February 2007 First Printing in Beijing, February 2007

ISBN 978-7-5022-3875-9

出版发行 原子能出版社(北京市海淀区阜成路 43 号 100037)

责任编辑 傅 真 王调霞

责任印制 丁怀兰 刘芳燕

印 刷 中国文联印刷厂

开 本 880 mm×1 230 mm 1/16

字 数 291.6 千字

印 张 9

版 次 2007 年 2 月第 1 版 2007 年 2 月第 1 次印刷

书 号 ISBN 978-7-5022-3875-9

经 销 全国新华书店

印 数 1—400 定 价 50.00 元

版权所有 侵权必究

**BEIJING NATIONAL
TANDEM ACCELERATOR LABORATORY**

Director Zhang Huanqiao
Vice Director Xia Haihong

**THE FIFTH ACADEMIC COMMITTEE
OF BEIJING NATIONAL TANDEM
ACCELERATOR LABORATORY**

Chairman Hu Renyu
Vice Chairman Chen Yongshou Guan Xialing
Secretary Jiang Shan

Committee Members

Physical Group

| | | |
|----------------|--------------|--------------|
| Liu Weiping | Ma Zhongyu | Fang Qinxue |
| Zhu Shengjiang | Zhu Shengyun | Xu Jincheng |
| Shen Wenqing | Zhang Benai | Zhu Lihua |
| Zhao Zhixiang | Guo Zhiyu | Guo Gang |
| Guo Shuling | Xu Shuwei | Chang Yongfu |

Accelerator Group

| | | |
|---------------|--------------|------------|
| Zhang Tianjue | Yang Bingfan | Zhao Kui |
| Xia Jiawen | Qin Jiuchang | Cui Baoqun |
| Fan Mingwu | | |

Specially Invited Committee Members

| | | | |
|-------------|--------------|------------|------------|
| Qi Zhanshun | Zhou Wenneng | Guo Yongji | Shi Qingyu |
|-------------|--------------|------------|------------|

Preface

The present progress report covers research and development activities using the HI-13 tandem accelerator at the Beijing National Tandem Accelerator Laboratory (BNTAL) for calendar year of 2005. During this period, the HI-13 tandem accelerator was operated smoothly and delivered ion beams over 4 000 hours, on the target, to the experiments in the fields of nuclear data measurement (20%), nuclear reaction (including nuclear astrophysics, 24%), nuclear structure (22%), and nuclear application (34%). Some main research progress was summarized as follows.

1 Nuclear Structure

The level schemes of ^{178}Os , ^{152}Gd , ^{137}La , ^{136}Ce , ^{106}Ag and ^{52}Mn were investigated and the half life of the levels was deduced. Signature inversion in doubly-odd nucleus ^{158}Tm was observed. Measurement of g -factors of magnetic dipole states in ^{85}Zr and measurement of ^7Be decay rate in Au were finished.

2 Nuclear Reactions

The excitation functions of quasielastic scattering at backward angles were measured for the system of $^{32}\text{S}+^{90,96}\text{Zr}$. The barrier distributions were extracted from these measured excitation functions. The measured barrier distribution of $^{32}\text{S}+^{96}\text{Zr}$ was broaden and extended to lower energy than in the case of $^{32}\text{S}+^{96}\text{Zr}$ due to the coupling of neutron transfer with positive Q -values, which resulted in a significant enhancement of fusion cross sections at the subbarrier energies.

3 Nuclear Astrophysics

The measurement of $^8\text{Li}(d, p)^9\text{Li}$ was used to deduce the S -factors of $^8\text{Li}(n, \gamma)^9\text{Li}$ and $^8\text{B}(p, \gamma)^9\text{C}$ reactions by ANC method. The reaction of $^{17}\text{F}(d, n)^{18}\text{Ne}$ was measured. Also, the ^{10}C secondary beam was produced. A setup for resonant scattering reactions with thick target was established.

4 Nuclear Data Measurement

We finished the measurement of double differential cross sections of $^6,7\text{Li}$ induced by fast neutrons. And the methodology study for neutron resonance parameter measurement within 0.1-1.0 MeV was made by using HI-13 tandem accelerator facility. Research on EUV spectra of highly ionized titanium and lifetime measurement of highly ionized ions were conducted.

5 Application of Nuclear Technology

By using accelerator mass spectrometry, traces of ^{129}I , ^{99}Tc , ^{41}Ca , ^{151}Sm and ^{79}Se were precisely measured. Radiation effects in various biological molecules and cells were investigated with ^7Li ion and protons beams. The single-event effects were calibrated for some important detectors and CMOS SRAM. Some properties of solid material surface modified by nuclear tracks were studied.

6 Theoretical Nuclear Physics

Calculations of electromagnetic transition probabilities and energy levels of the doublet bands in ^{134}Pr were carried out with triaxial projected shell model and lead to a conclusion that the observed nearly degenerate doublet bands in ^{134}Pr can not be interpreted as chiral bands. Relativistic microscopic optical potential of the nucleon scattering off nuclei was investigated in the framework of the Dirac Brueckner-Hartree-Fock approach. A special attention was paid to the isospin dependence of the nucleon effective interaction and effective mass. The dynamic calculation of heavy ion fusion was applied to study of super heavy element.

7 Academic Exchange

The academic exchange has been enhanced year by year. The tandem beam time about 2 000 hours was provided to outside users such as Peking University, Tsinghua University, Jilin University and Institute of Modern Physics etc. For all users, the publication of SCI papers was about 50 per year.

The Tandem Upgrading Project, or Beijing Radioactive Ion-beam Facility (BRIF), was approved. A construction contract was signed to build a 100 MeV, 200 μA compact proton cyclotron. The cyclotron design started in this year.

Finally, I would like to thank all of scientists, technicians and administration stuffs for their great contribution to the progress of this laboratory.

Director



Department of Nuclear Physics, CIAE

December 6, 2006

CONTENTS

Theoretical Nuclear Physics

- 1 Misleading Chiral Bands in ^{134}Pr Chen Yongshou, et al (3)
- 2 Signature Inversion as a Probe for Triaxial Rotation Chen Yongshou, et al (5)
- 3 Theoretical Study on the $^2\text{H}(\text{d}, \gamma)^4\text{He}$ Reaction Below $E_{\text{c.m.}} < 3$ MeV Ma Yinqun, et al (8)
- 4 Nucleon Effective Mass in Dirac Brueckner-Hartree-Fock Approach Ma Zhongyu, et al (10)
- 5 Pigmy Dipole Mode in $^{26,28}\text{Ne}$ in the Quasiparticle Relativistic Random Phase Approximation
..... Cao Ligang, et al (15)
- 6 Isospin-Dependent Optical Potentials in Dirac Brueckner Hartree-Fock Approach
..... Rong Jian, et al (19)
- 7 Applications of Skyrme Energy-Density Functional to Fusion Reactions for Synthesis of Superheavy
Nuclei Wang Ning, et al (22)
- 8 Applications of Skyrme Energy-Density Functional to Fusion Reactions Spanning the Fusion Barriers
..... Liu Min, et al (24)
- 9 Investigation in Possibility of Producing Superheavy Fragments Through Massive Nuclear Reactions
at Low Energies Wu Xizhen, et al (25)
- 10 Effects of Isospin Equilibrium on Cold Fusion of Superheavy Nuclei Liu Zuhua (26)
- 11 Application of the Self-Consistent Collective Coordinate Method to Multi-O(4) Model
..... Gu Jianzhong (29)

Experimental Nuclear Physics

- 1 The Astrophysical ^8Li (n, γ) ^9Li Reaction Rate Li Zhihong, et al (33)
- 2 A Setup for Resonant Scattering Reactions With Thick Target Wang Youbao, et al (35)
- 3 Measurement of $^{17}\text{F}(\text{d}, \text{n})^{18}\text{Ne}$ reaction Yan Shengquan, et al (37)
- 4 Determination of Astrophysical Reaction Rate of $^8\text{Li}(\text{d}, \text{p})^9\text{Li}$ Guo Bing, et al (39)
- 5 Astrophysical S -Factor for $^8\text{B}(\text{p}, \gamma)^9\text{C}$ via a Study of the $^8\text{Li}(\text{d}, \text{p})^9\text{Li}$ Reaction ... Guo Bing, et al (41)
- 6 Production of ^{10}C Secondary Beam Su Jun, et al (43)
- 7 Study of Neutron Emission Reactions of $^6,7\text{Li}$ Induced by Fast Neutrons Ruan Xichao, et al (45)
- 8 Double-Differential Neutron Emission Cross Sections Measurements and Theoretical Analysis of $^6,7\text{Li}$
at Incident Neutron Energies of 8.17 and 10.27 MeV Chen Guochang, et al (48)
- 9 The Methodology Study for Neutron Resonance Parameter Measurement Within 0.1-1.0 MeV by
Using HI-13 Tandem Accelerator Facility Li Xia, et al (55)
- 10 Partial Fusion Induced by Weakly Bound Projectiles Liu Zuhua, et al (58)
- 11 Study of Barrier Distributions for $^{32}\text{S}+^{90,96}\text{Zr}$ Yang Feng, et al (60)
- 12 An Experimental Study on Long-Range Angular Correlation in Excitation Functions for the Reaction
System of $^{19}\text{F}+^{27}\text{Al}$ Wang Qi, et al (61)
- 13 Identification of Band Structures in ^{137}La Zhu Shengjiang, et al (62)
- 14 High Spin States in ^{136}Ce Zhu Shengjiang, et al (65)
- 15 The High Spin Structures of the Odd-Odd Nucleus ^{106}Ag He Chuangye, et al (68)
- 16 Structure of High Spin States in ^{52}Mn Wu Xiaoguang, et al (70)
- 17 Lifetime Measurement of the High Spin States in ^{178}Os Wu Xiaoguang, et al (71)

| | | |
|----|--|-------------------------|
| 18 | Signature Inversion in Doubly-Odd Nucleus ^{158}Tm | Ma Yingjun, et al (73) |
| 19 | High-Spin States in ^{152}Gd | Hua Hui, et al (76) |
| 20 | Measurement of g -Factors for Magnetic Rotational Band in ^{85}Zr | Yuan Daqing, et al (77) |
| 21 | Precise Measurement of ^7Be Decay Rate in Au | Li Chengbo, et al (78) |
| 22 | Research on EUV Spectra of Highly Ionized Titanium | Yang Zhihu, et al (80) |
| 23 | Study of the Lifetime of Highly Ionized Atoms | Du Shubin, et al (83) |

Applications of Nuclear Physics

| | | |
|----|---|---------------------------|
| 1 | ^{99}Tc Measurement With Accelerator Mass Spectrometry at China Institute of Atomic Energy | He Ming, et al (87) |
| 2 | Study on $^{41}\text{CaF}_2$ AMS Analytical Method and Skeletal Calcium Metabolism by ^{41}Ca Tracing | Li Shihong, et al (92) |
| 3 | Measurement of Trace ^{129}I Concentrations in Neutrino Detector Material With Accelerator Mass Spectrometry | Dong Kejun, et al (94) |
| 4 | Measurement Method of ^{151}Sm and ^{79}Se With AMS | Yin Xinyi, et al (96) |
| 5 | The Primary Study of Radiation Effect of Biology Induced by Protons | Yue Maoxing, et al (98) |
| 6 | Investigation of DNA Damage Induced by Direct and Indirect Effects of ^7Li Ions Radiation | Sui Li, et al (100) |
| 7 | DNA End-Joining Catalyzed by Cell-Free Extracts After Heavy Ions Irradiation | Kong Fuquan, et al (102) |
| 8 | Bio-effects of ^7Li Ion Beams Irradiation on Wheat | Liu Luxiang, et al (104) |
| 9 | DC/DC High Energy Proton Radiation Test | Yu Qingkui, et al (105) |
| 10 | The Accelerator Calibration of Single-Event Detector of FY-3 | Wang Shijing, et al (106) |
| 11 | The Accelerator Calibration of High-Energy Proton Detector and Heavy-Ion Detector of the Double-Star Project | Wang Shijing, et al (107) |
| 12 | Identification of SEU Sensitive Region of CMOS SRAM Using Heavy Ion Microbeam | Guo Gang, et al (108) |
| 13 | Study on Properties of Solid Material Surface Modified by Nuclear Tracks | Liu Cunxiong, et al (110) |
| 14 | Nuclear Recoiled Quenching Factor Measurement for a HPGe Detector Using a Monoenergetic Neutron Beam | Ruan Xichao, et al (111) |

Accelerator and Detector

| | | |
|---|--|--------------------------|
| 1 | Preparative Technologies for Three-Layer-Sandwich Targets Used by Measuring g -Factor of Rotational Levels | Fan Qiwen, et al (117) |
| 2 | Preparation of Self-Supporting Targets With Thickness of Less Than $100\text{ }\mu\text{g}/\text{cm}^2$ by Focused Heavy-Ion Beam Sputtering | Fan Qiwen, et al (119) |
| 3 | HI-13 Tandem Accelerator in 2005 | Kan Chaoxin, et al (121) |

Appendix

| | | |
|---|--|------------------|
| 1 | List of Scientific Publications Issued in 2005..... | (125) |
| 2 | International Scientific Technology Exchanges | (130) |
| 3 | The Statistics of Tandem Accelerator Beam Time in the Past Years | Hu Yueming (136) |

THEORETICAL NUCLEAR PHYSICS

1 Misleading Chiral Bands in $^{134}\text{Pr}^*$

Chen Yongshou, Gao Zaochun

(China Institute of Atomic Energy, P. O. Box 275-18, Beijing 102413, China)

The chirality is common and has important consequence in science. Many biological and pharmaceutical molecules have static chirality when they are composed of four different atoms. The chirality may exist in nuclei when a particular angular momentum coupling scheme appears, where three angular momenta of the valence neutrons, the valence protons and the core are mutually perpendicular so that a left- and a right-handed systems can be formed. The possibility was considered recently, following the observation of doublet bands built on the intrinsic configuration of $\pi h_{11/2} \otimes \nu h_{11/2}$ in the $A=130$ mass region. ^{134}Pr is known as a best candidate where the nearly degenerate doublet bands were found experimentally. The energy degeneracy of doublet band states with the same spin and parity is an important indication for the occurrence of chirality. Among other things, however, the most crucial criteria for the chirality are the equivalence of the reduced E2 transition probabilities in the doublet bands. Very recently, the decisive experiment of measuring electromagnetic transition rates have been done, and a large difference of the experimental $B(E2)$ values for the doublet bands of ^{134}Pr has been reported^[1]. Then a serious question arises whether the observed doublet bands in ^{134}Pr can be characterized as having chirality, and this is the issue that underlies the present investigation. To answer this question we carried out calculations of electromagnetic transition probabilities and energy levels of the doublet bands with triaxial projected shell model (TPSM) which has been recently developed in CIAE.

The shell model Hamiltonian, involving a large number of nucleons moving in a spherical Nilsson potential and an interaction of separable multipole $Q \cdot Q$ forces plus monopole pairing plus quadrupole pairing, is written as

$$H = H_0 - \frac{1}{2} \sum_{\lambda=2}^4 \chi_{\lambda} \sum_{\mu=-\lambda}^{\lambda} Q_{\lambda\mu}^+ Q_{\lambda\mu} - G_0 P_{00}^+ P_{00} - G_2 \sum_{\mu=-2}^2 P_{2\mu}^+ P_{2\mu} \quad (1)$$

The wave function is given by

$$|\Psi_{\text{IM}}^{\sigma}\rangle = \sum_{K\kappa} f_{\text{IK}\kappa}^{\sigma} \hat{P}_{\text{MK}}^I |\phi_{\kappa}\rangle \quad (2)$$

where the three-dimensional angular momentum projection operator is written as

$$P_{\text{MK}}^I = \frac{2I+1}{8\pi^2} \int d\Omega D_{\text{MK}}^I(\Omega) \hat{R}(\Omega) \quad (3)$$

and $|\phi_{\kappa}\rangle$ represents a set of triaxially deformed BCS multi-quasiparticle states. By solving the Hamiltonian equation

$$H |\Psi_{\text{IM}}^{\sigma}\rangle = E^{\sigma}(I) |\Psi_{\text{IM}}^{\sigma}\rangle \quad (4)$$

we obtain energies $E^{\sigma}(I)$ of states “ σ ” as a function of spin I , together with wave functions $f_{\text{IK}\kappa}^{\sigma}$. The

reduced rate of electromagnetic transitions between the eigenstates $|\Psi_{IM}^\sigma\rangle$, induced by a spherical tensor operator $\widehat{M}_{\lambda\mu}$, is

$$B(M\lambda; i \rightarrow f) = \frac{2I_f + 1}{2I_i + 1} \left| \langle \Psi_{I_f}^{\sigma_f \pi_f} \| \widehat{M}_\lambda \| \Psi_{I_i}^{\sigma_i \pi_i} \rangle \right|^2 \quad (5)$$

and the reduced matrix elements become

$$\begin{aligned} \langle \Psi_{I_f}^{\sigma_f \pi_f} \| \widehat{M}_\lambda \| \Psi_{I_i}^{\sigma_i \pi_i} \rangle &= \frac{1}{2} (1 + \pi_f \pi_i \pi_\lambda) \sum_{K_i K_f \kappa_f} f_{I_f K_f \kappa_f}^{\sigma_f \pi_f} f_{I_i K_i \kappa_i}^{\sigma_i \pi_i} \\ &\sum_{\mu} \langle I_i K_f - \mu \lambda \mu | I_f K_f \rangle \langle \phi_{\kappa_f} | \widehat{M}_{\lambda\mu} P_{K_f - \mu K_i}^{I_i \pi_i} | \phi_{\kappa_i} \rangle \end{aligned} \quad (6)$$

The calculated band energies are compared with experimental data and shown in Fig.1, and it is seen that a good agreement between theory and experiment has been achieved. Particularly, the crossing behavior of the band 1 (yrast) and the band 2 (nonyrast) was reproduced by the present calculation. At the nearly degenerate region, from $I=14$ to 17, calculated $B(E2)$ values are larger for band 1 than for band 2 by a factor of 3, in average, see Fig.2, and this is in a nice agreement with the experimental $B(E2)$ data^[1]. Detailed analysis for the intrinsic structures of calculated doublet bands indicates that from spin $I=14$ to 18 the doublet bands have completely different nature, namely the band 1 is built on a 2 quasiparticle (q.p.) state, $1n1p$, while the band 2 is mainly built on a 4 q.p. one, $1n3p$. The shell model configuration mixing of 4 q.p. component gives rise to a strong reduction of $B(E2)$ values of the band 2 in the band interaction region, $I=14$ to 17. The chiral doublet bands should have a similar intrinsic structure, therefore our theoretical results lead to a conclusion that the observed nearly degenerate doublet bands in ^{134}Pr can not be interpreted as chiral bands.

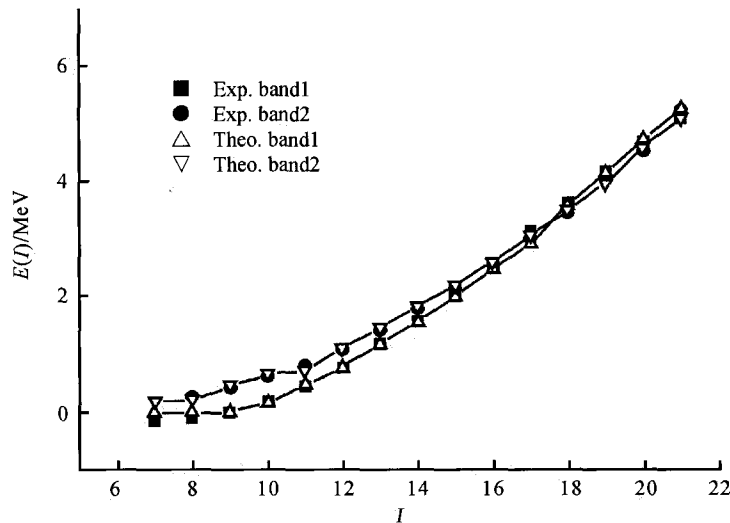


Fig. 1 Calculated and experimental energy levels of the chirality candidate bands of ^{134}Pr

The experimental data was taken from reference [1]

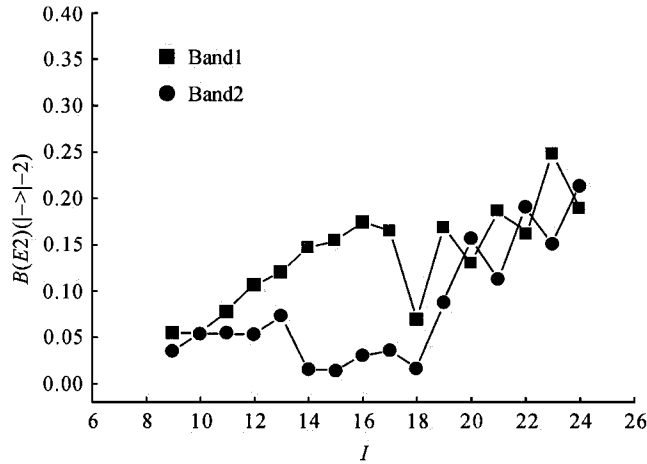


Fig. 2 Calculated $E2$ transition probabilities of the chirality candidate bands of ^{134}Pr

Reference

- [1] Tonev D, et al. Phys Rev Lett, 2006, 96: 052 501.

* Supported by National Natural Science Foundation of China (10305019, 10475115, 10435010), and Major State Basic Research Development Program of China (G20000774)

中文摘要

原子核中也可能存在手征性, ^{134}Pr 被认为是最好的候选者, 因为在此核中实验上发现了近似简并的二重带。然而, 手征性最关键的判据并不是能量的简并, 而是二重带的带内 $E2$ 跃迁概率要基本相同。新近的实验测量表明, 此二重带的 $B(E2)$ 实验值与报道值很不相同。这样, ^{134}Pr 二重带的手征性质就成了大问题。为了回答这个问题, 我们发展三轴投影壳模型, 计算了此二重带的电磁跃迁概率和能级, 计算结果很好地再现了实验数据。深入分析表明, 在 $I=14$ 到 18 区间, 二重带具有完全不同的性质, 因此, ^{134}Pr 二重带不能解释为手征带。

2 Signature Inversion as a Probe for Triaxial Rotation*

Chen Yongshou, Gao Zaochun

(China Institute of Atomic Energy, P. O. Box 275-18, Beijing 102413, China)

The signature inversion phenomenon has been widely observed in nuclear rotational spectra but has no common understanding for more than 20 years. The signature inversion is strongly related to the triaxial rotation, while how a triaxially deformed nucleus rotates is a fundamental question in nuclear structure. The present study attempts to achieve a thorough explanation for the signature inversion and to

provide the rules to probe the rotation of triaxial nuclei by examining experimental signature inversion data. The signature is associated with the invariance of a system with intrinsic quadrupole deformation under a rotation of 180° around a principal axis, and is defined in the cranking model. We define the dynamic cranking axis as the axis along which the total angular momentum has a largest component. Note that the dynamic cranking axis can be any one of three principal axes of a rotating triaxial nucleus, while the cranking axis defined in the cranking model is a fixed one. We interpret the signature inversion as the change of the dynamic cranking axis in the rotational triaxial nuclear system. Take the yrast band of odd proton nucleus ^{157}Ho as an example, where the twice signature inversions were observed experimentally at spin $I=37/2$ and $53/2$ respectively^[1]. This band is based on an intrinsic configuration of the Fermi aligned proton orbital in the proton $h_{11/2}$ shell, namely the proton Fermi level lies in the middle of the shell, which has a large alignment component I_y along the y -axis, the intermediate axis, thus the occurrence of the signature inversion in the band is mainly determined by the characteristic of the y -axis, namely as the dynamic cranking axis or not. In order to investigate the double signature inversion and explore the triaxial rotation the quantity $S(I)=E(I)-E(I-1)$ for the yrast band of ^{157}Ho was calculated with the triaxial projected shell model (TPSM) which has recently been developed in CIAE as an extension of RASM. The shell model Hamiltonian, involving a large number of nucleons moving in a spherical Nilsson potential and an interaction of separable multipole $Q \cdot Q$ forces plus monopole pairing plus quadrupole pairing, is written as

$$H = H_0 - \frac{1}{2} \sum_{\lambda=2}^4 \chi_\lambda \sum_{\mu=-\lambda}^{\lambda} Q_{\lambda\mu}^+ Q_{\lambda\mu} - G_0 P_{00}^+ P_{00} - G_2 \sum_{\mu=-2}^2 P_{2\mu}^+ P_{2\mu} \quad (1)$$

The wave function is given by

$$|\Psi_{\text{IM}}^\sigma\rangle = \sum_{K\kappa} f_{\text{IK}\kappa}^\sigma \hat{P}_{\text{MK}}^I |\phi_\kappa\rangle \quad (2)$$

where the three-dimensional angular momentum projection operator is written as

$$P_{\text{MK}}^I = \frac{2I+1}{8\pi^2} \int D_{\text{MK}}^I(\Omega) \hat{R}(\Omega) d\Omega \quad (3)$$

and $|\phi_\kappa\rangle$ represents a set of triaxially deformed BCS multi-quasiparticle states. By solving the Hamiltonian equation

$$H |\Psi_{\text{IM}}^\sigma\rangle = E^\sigma(I) |\Psi_{\text{IM}}^\sigma\rangle \quad (4)$$

We obtain energies $E^\sigma(I)$ of states “ σ ” as a function of spin I , together with wave functions $f_{\text{IK}\kappa}^\sigma$. The expectation values of the components of total angular momentum along the three intrinsic principal axis can be calculated by using the eigenstate wave function $|\Psi_{\text{IM}}^\sigma\rangle$. The calculated results quite well reproduce the double signature inversions observed in ^{157}Ho , as shown in Fig.1. Detailed calculations show that the first signature inversion is caused by the change of the dynamic cranking axis from the y - to the x -axis, while the second inversion is due to the change back of the dynamic cranking axis to the y -axis from the x -axis, the shortest axis (Fig.2). The cause of the dynamic axis change may be attributed to the alignments of the pair of neutrons in the $i_{13/2}$ shell. The mechanism for signature inversion provided in the

present study is general, can be applied to, for example, odd-odd nuclei $^{120-130}\text{Cs}$, where the dynamic cranking axis is the x -axis at low spins and becomes the y -axis after the inversion spin^[2].

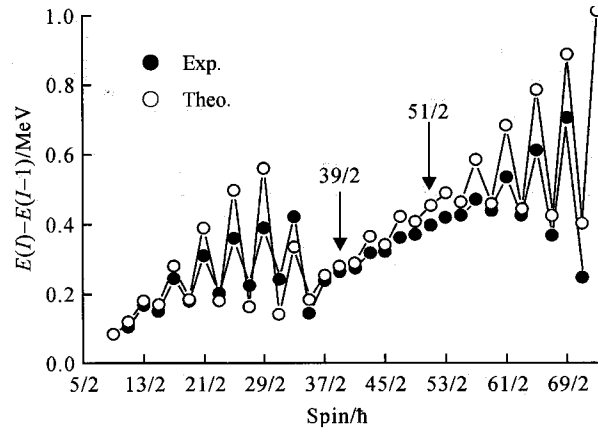


Fig. 1 Calculated energies $E(I) - E(I-1)$ of the yrast band states for ^{157}Ho , compared with the experimental data
Arrows indicate the signature reversion point

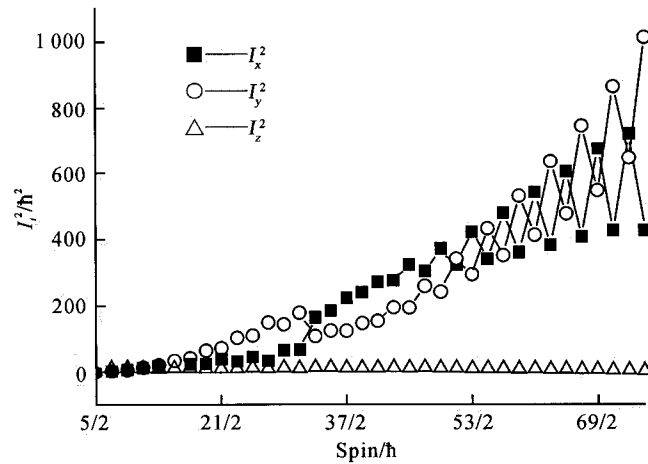


Fig. 2 Calculated expectation values of I_x^2 , I_y^2 and I_z^2 with the wave functions that has reproduced the double signature inversions in Fig.1

References

- [1] Hagmann B, et al. Nucl Phys, 1984, A424: 365.
- [2] Gao Zaochun, Chen Yongshou, Yang Sun. Phys Lett, 2006, B634: 195.

* Supported by National Natural Science Foundation of China (10305019, 10475115, 10435010), and Major State Basic Research Development Program of China (G20000774)

中文摘要

二十多年来, 旋称反转现象在核转动谱中被大量地观测到, 但没有统一的认识。本研究试图对旋称反转给出完全的解释, 并提出由旋称反转实验数据出发分析三轴形变核转动的规律。我们定义动力学推转轴为总角动量在其上有最大分量之轴, 我们解释旋称反转为三轴转动核中动力学推转轴的改变。

3 Theoretical Study on the $^2\text{H}(\text{d}, \gamma)^4\text{He}$ Reaction Below $E_{\text{c.m.}} \leq 3 \text{ MeV}$

Ma Yinqun^{1,2}, Ma Zhongyu¹

(1. China Institute of Atomic Energy, P. O. Box 275-18, Beijing 102413, China;

2. Physics Department, Taiyuan Normal University, Taiyuan 030001, China)

The quantitative Cosmology is becoming a valid description of modern models of the early universe. The results deduced from the prediction of big-bang nucleosynthesis (BBN), combined with the latest Cosmic Microwave Background anisotropy measurements, give independent and accurate predictions of the baryon density and can be used to test the standard cosmology framework. The abundances of the light nuclei, ^2H , ^3He , ^4He and ^7Li have been used to test the consistency of the hot big-bang model at early (first 10^3 seconds) stages of evolution of the universe. To construct the BBN reaction network, the astronomical measurements of the light element abundances need to be complemented by the reaction rate knowledge in the relevant energy region (from few tens to few hundreds of keV). The deuteron- deuteron radiative capture reaction is one of the deuterium-burning processes for which the cross section is not well known at very low energies. For the reaction $^2\text{H}(\text{d}, \gamma)^4\text{He}$ due to extremely low reaction rates at the astrophysically important energies (about below few hundreds of keV), the relevant cross section data are impractically obtained for direct laboratory measurements. The present study was undertaken to obtain ones.

We present a phenomenological study of the $^2\text{H}(\text{d}, \gamma)^4\text{He}$ reaction that allows for the D-state component of the colliding deuterons. In the L-S coupling states of the d-d system may have the following possible states with lowest angular momenta: 3S_0 , 5S_2 , $^3P_{0,1,2}$, 1D_2 . Considering electromagnetic radiation with multipolarity less than 2, the following transitions are allowed:

$$\langle ^4\text{He} | E2 | ^5S_2 \rangle, \langle ^4\text{He} | E2 | ^1D_2 \rangle$$

The wave function of the d-d system can be expressed as produces of internal deuteron wave functions Φ_d^S and a relative motion $f(R)$,

$$\psi(^{2S+1}L_J) = \frac{f_{LS}^J(R)}{R} [Y_L(\hat{R})(\Phi_d^{S_1=1} \Phi_d^{S_2=1})_S]_J \quad (1)$$

Considering D-state components in ^4He , the ground state of ^4He could be expressed as

$$\psi_\alpha = \cos \omega \psi(^1S_0) + \sin \omega \psi(^5D_0) \quad (2)$$

where the radial wave functions are normalized to one. The mixing angular ω parameterizes the D-state amplitude in ^4He . The scattering wave functions of the d-d system are,

$$\psi = i^L \left(\frac{4\pi(2L+1)}{v} \right)^{1/2} \frac{1}{k} \psi(^{2S+1}L_J) \quad (3)$$

where L is the orbital angular momentum, S the channel spin, and J the total angular momentum. v and k are relative velocity and wave number of the colliding deuterons. The scattering wave functions are normalized to unit flux.

We simply display our results for the capture cross section

$$\sigma(E_{\text{c.m.}}) = \sum_{S=0,2} \frac{4\pi}{75} \frac{2S+1}{45} \left(\frac{E_\gamma}{\hbar v} \right)^5 \frac{1}{k^2} \frac{e^2}{\hbar v} |A(^{2S+1}L_J)|^2 \quad (4)$$

where $E_\gamma = E_{\text{c.m.}} + 23.847$ MeV is the energy of the emitted photon, $A(^{2S+1}L_J)$ is the transition amplitude. As mentioned above, we will adjust ω to reproduce the absolute normalization of the low energy experimental cross section. At low energies, it is most convenient to present the data in terms of the astrophysical S -factor, defined by

$$S(E_{\text{c.m.}}) = \sigma(E_{\text{c.m.}}) E_{\text{c.m.}} \exp(2\pi\eta) \quad (5)$$

where $\eta = e^2/\hbar v$ is the Sommerfeld parameter. The radial wave functions in ^4He are calculated in Woods-Saxon potentials, which parameters are adjusted to reproduce the d-d break up energies of ^4He and low energy d-d elastic phase shifts, respectively. The parameters in our calculations are given in table 1. We can well reproduce the energy dependence of the S -factor if we choose $\omega = -0.275$ for the potential leading to a ^4He D-state probability of $P_D = 7.4\%$, and theoretical results are compared with the experimental data in Fig.1. The agreement with the experimental data at $E_{\text{c.m.}} \leq 3$ MeV is very satisfactory. We extend our model to the energy range $E_{\text{c.m.}} \leq 50$ keV, which is important for the ^4He nucleosynthesis during the big bang. Our S -factor is nearly linear in energy: $S(E_{\text{c.m.}}) \approx S_0 + S_1 E_{\text{c.m.}}$ and can be well approximated with the coefficients $S_0 = 6.29 \times 10^{-6}$ keV·b and $S_1 = -1.14 \times 10^{-8}$ b.

Table 1 Woods-Saxon parameters used in theoretical calculations

| States | V_0/MeV | R_0/fm | a/fm | R_f/fm | E_b/MeV |
|---------|------------------|-----------------|---------------|-----------------|------------------|
| 1S_0 | -48.284 | 2.96 | 0.9 | 1.83 | -23.847 |
| 5D_1 | -100.413 | 2.96 | 0.9 | 1.83 | -23.847 |
| 5D_2 | 15.4 | 2.96 | 0.9 | 1.83 | |
| 1D_2 | -16.5 | 2.96 | 0.9 | 1.83 | |